JOURNAL OF GEOPHYSICAL RESEARCH, VOL. 105, NO. D15, PAGES 20,131–20,143, AUGUST 16, 2000

Parameter estimation of GOES precipitation index at different calibration timescales

Liming Xu, Xiaogang Gao, Soroosh Sorooshian, and Bisher Imam

Department of Hydrology and Water Resources, University of Arizona, Tucson

Abstract. We examined two techniques that adjust the parameters of the GOES Precipitation Index (GPI) by combining the polar microwave and the geosynchronous infrared observations at three frequencies: daily, pentad, and monthly. The first technique is the adjusted GPI (AGPI), and the second is the universally adjusted GPI (UAGPI). The study shows that rainfall estimates can be improved by frequent calibrations providing there is sufficient superior (microwave) rainfall sampling within the calibration time and space domain. For this work, daily and pentad calibrations produce monthly rainfall estimates almost as good as monthly calibration. The daily calibration produced better daily rainfall estimates than pentad and monthly calibration, but it generates similar pentad rainfall estimates to these of the pentad calibration. The monthly calibrated scheme is not suitable for the daily and pentad rainfall estimates. Under the current twice-per-day sampling rate of polar-orbiting microwave observations, the pentad calibration scheme is suggested for the monthly, pentad, and daily rainfall. The potentials of applying the UAGPI and the AGPI techniques for daily rainfall estimation are also investigated.

1. Introduction

Satellite precipitation estimation is indispensable to global climate and hydrological studies because of the lack of precipitation data from traditional measuring instruments over oceans and remote continental regions. Although a large number of satellite rainfall algorithms have been developed over the past three decades using various satellite observations, it is generally agreed that a combination of microwave data from polar-orbiting satellites and infrared data from geosynchronous platforms is a potential way to improve global rainfall estimates in terms of accuracy and temporal/spatial resolution [*Simpson et al.*, 1996]. On the one hand, the infrared (IR) imager only observes the cloud-top brightness temperature, and the microwave images can penetrate through the cloud columns and expose more physical information about precipitation, especially over oceans where the background surface emission is low and uniform. On the other hand, the sampling (scanning) rate of the IR sensor from GOES (approximately 1/2 hourly) is much higher than that of the microwave sensor from the polar-orbiting satellite (twice a day) and is able to monitor the spatial and dynamic variation of the cloud field. Several methods have been proposed to take advantage of the microwave instantaneous rain estimates and the high resolution of IR data to improve monthly rainfall estimates [*Adler et al.*, 1993, 1994; *Xu*, 1997] by calibrating the (GPI) parameters using microwave rainfall estimates.

GPI is an IR rainfall estimation algorithm which includes two model parameters: (1) an IR brightness temperature threshold that identifies rain pixels and (2) a constant mean rain rate that is assigned to each of the rain pixels. These parameters were originally calibrated to 235°K and 3.0 mm h^{-1} over a region in the eastern tropical Atlantic Ocean during the Global Atmosphere Research Program (GARP) Atlantic Tropical Experiment [*Arkin*, 1979; *Arkin and Meisner*, 1987]. The calibrated parameters were obtained by regressing the 6-hourly radar-estimated rainfall against 6-hourly fractional IR cloud coverage colder than 235°K over 2.5° × 2.5° grids. These parameters were then applied to produce global monthly rainfall estimates as one of the basic algorithms for the Global Precipitation Climatology Project (GPCP) [*Arkin and Ardanuy*, 1989; *Huffman et al.*, 1997]. Although GPI has generally outperformed many other algorithms in several algorithm intercomparison projects for monthly rainfall estimation, GPI suffers from inconsistent performance when applied to areas away from tropical oceanic regions [*Ebert et al.*, 1996]. As expected, GPI lacks the ability to accurately delineate rain coverage areas and to make rainfall estimates at higher resolutions due to the significant amount of no-rain cold clouds misidentified as rain clouds by the temperature threshold [*Arkin and Xie*, 1994]. However, GPI substantiates two important parameters with physical concepts for the satellite rainfall estimate, namely, the rain pixel and mean rain rate. Indisputably, the spatial and temporal variations of rainfall fields require the change of the two parameters over time and region for more accurate rainfall estimates.

Adler et al. (1993, 1994) developed a method of adjusting the GPI mean rain rate according to microwave rainfall estimates at the moments when IR and microwave observations are both available, while the GPI threshold was kept the same. This method is termed as the adjusted GPI (AGPI). A method of changing both GPI parameters was also proposed [*Xu*, 1997]. The IR temperature threshold is computed to make the area of IR-estimated rain pixels the same as that of microwave rain pixels, and the rain rate is equal to the mean microwave rain rate in a grid. Both

Paper number 2000JD900178.
0148-0227/00/2000JD900178$09.00

parameters are calibrated locally for each grid. This method is termed as the universally adjusted GPI (UAGPI). The fundamental theme of these algorithms is to calibrate GPI parameters with superior microwave rainfall estimates, and such calibration can be carried out in various time intervals such as monthly, pentad, and daily. For wide applications, studies are needed to answer two questions: (1) Is combining techniques like the UAGPI and the AGPI capable of making rainfall estimates at the temporal resolutions higher than monthly? (2) What calibration frequencies are required in rainfall estimates at various temporal resolutions?

2. Data Description

Two data sets were used to examine the effects of various calibration schemes on rainfall estimates. The first data set is the one used in the First Algorithm Intercomparison Project (AIP-1) initiated by the Global Precipitation Climatology Project (GPCP) of the World Climate Research Program [*Lee et al.*, 1991]. The second one is the data set used by the Third Algorithm Intercomparison Project (AIP-3).

2.1. AIP-1 Data Set

This data set covers two month-long periods in 1989: June 1-30 (hereinafter referred to as the June data set) and July 15 to August 15 (hereinafter referred to as the July/August data set) over the Japanese Islands and adjacent oceanic areas (Figure 1). The data set includes IR, visible, and multichannel microwave satellite images as well as ground-observation rainfall fields. IR and visible imagery data were observations made by the Japanese Geostationary Meteorological Satellite (GMS), reprocessed to a spatial resolution of 0.25° × 0.25° latitude by longitude. Microwave data were measured by the Special Sensor Microwave/Imager (SSM/I) instruments aboard the DMSP (Defense Meteorological Satellite Program) series of sun-synchronous, polar-orbiting platforms. The ground-observation rainfall data, in the form of radar-rain-gage composite, were assembled by the Japanese Meteorological Agency (JMA) through radar and high-density rain gage networks. Both microwave rainfall estimates and radar-rain-gage rainfall were reprocessed to match the IR spatial resolution of 0.25° × 0.25°. From now on, a 0.25° × 0.25° image unit will be called a pixel, and a 1.25° × 1.25° area containing 25 pixels will be called a grid cell in order to be consistent with the spatial resolution used in AIP-1. The IR and visible satellite images, as well as radar-rain-gage composite rainfall, are hourly data, while the SSM/I observations covered the study area twice a day at most.

2.2. AIP-3 Data Set

AIP-3 made use of the data collected during the intensive observing period of the Tropical Ocean-Global Atmosphere Coupled Ocean-Atmosphere Response Experiment (TOGA COARE), which took place from November 1992 to February 1993 [*Ebert et al.*, 1996]. Radar rainfall measurements over the equatorial western Pacific warm pool were obtained by two shipboard Doppler radar. The rainfall data used in this research were generated from the Version 2 algorithms which increased overall rain rates by 30-40% over the Version 1 release for an adjustment of the radar calibration problem. The satellite IR data were taken from the GMS observations. Both rainfall and IR data were reprocessed to a spatial resolution of 0.25° × 0.25°. Grid resolution was chosen to be 1° × 1° consistent with the AIP-3 project. The study area

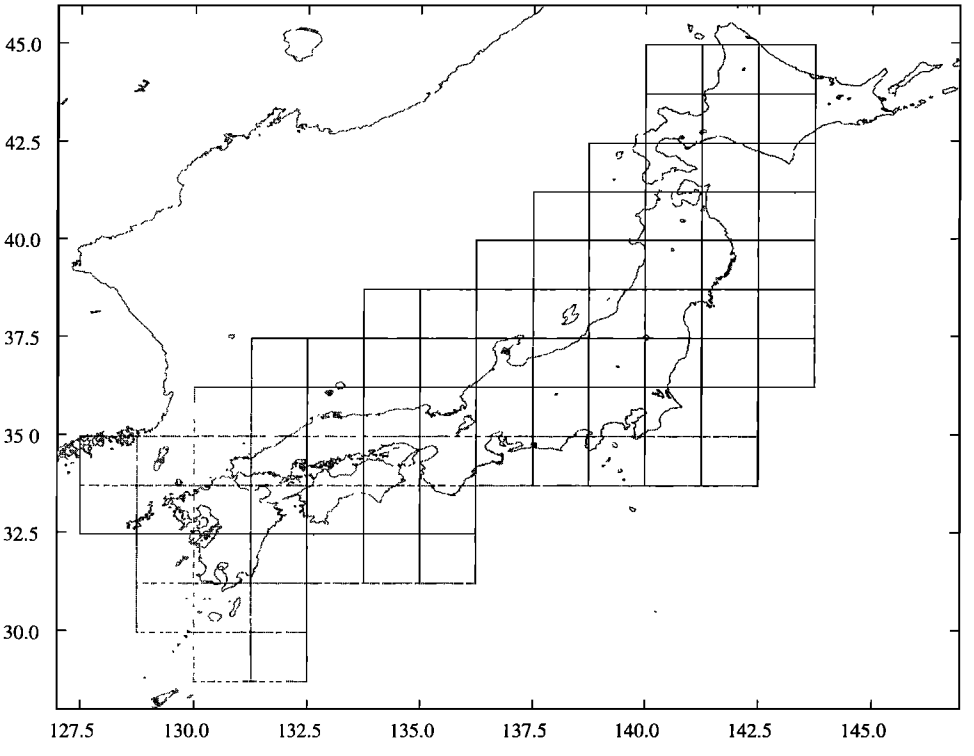

Figure 1. First Algorithm Intercomparison Project (AIP-1) study area of Japanese Islands and adjacent oceanic area. The frame indicates the radar coverage area and each square represents a 1.25° × 1.25° grid cell.

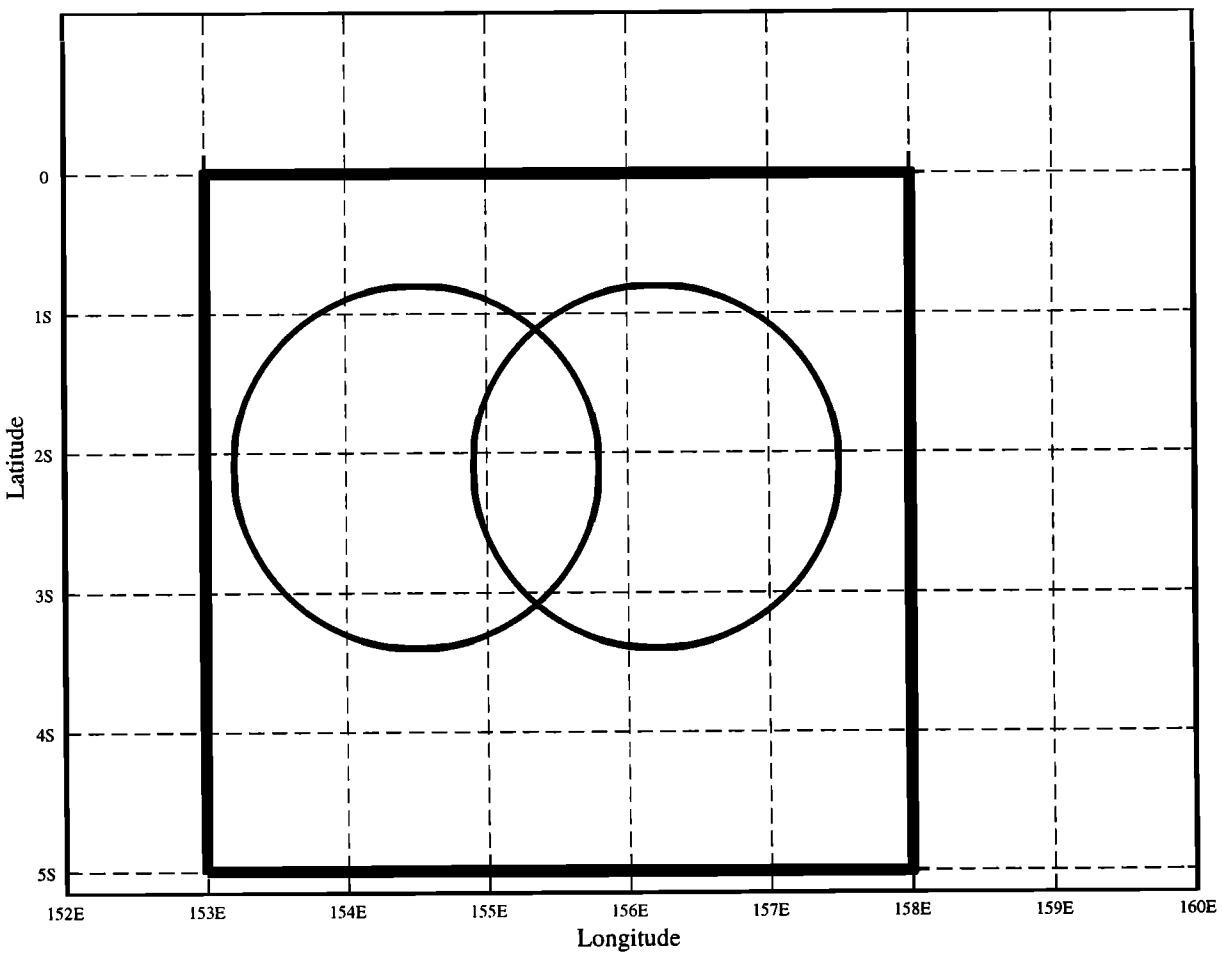

Figure 2. AIP-3 study area from Tropical Ocean-Global Atmosphere Coupled Ocean-Atmosphere Response Experiment (TOGA COARE). Two circles represent the shipboard radar coverage areas.

covers approximately 400 km (E-W) by 300 km (N-S) centered near 2°S, 156°E (Figure 2). Moreover, the data in month 2 (December 15, 1992 to January 18, 1993) and month 3 (January23, to February 23, 1993) were used in this research because these months contain most of the rainfall for the AIP-3 study period.

3. Methods

Because the purpose of this research is to study the effectiveness of techniques of combining IR and microwave data for rainfall estimation, we will use the radar-rain-gage composites to simulate the microwave rainfall estimates. In other words, we replaced the microwave rainfall estimates with radar rainfall observations at times when SSM/I satellite overpasses the study region. Therefore the algorithm errors of microwave rainfall estimates would not mingle with sampling errors, whose reduction was the main purpose of developing algorithms like the AGPI and UAGPI. The algorithm errors of current microwave techniques are so high that it is difficult to detect the effectiveness for various combination techniques if microwave rainfall estimates are used for the combination [*Ferraro and Mark*, 1995; *Xu et al.*, 1999]. The microwave rainfall estimates will be referred to hereinafter as the radar-rain-gage composite-simulated microwave observations. For the purpose of eliminating the effects of partial-grid coverage on the edges of a microwave swath, we simply took two 12-hour-apart radar-gage composite rainfalls over the whole study area to mimic the microwave rain estimates.

3.1. Algorithms

3.1.1. AGPI algorithm. The algorithm modifies the GPI rainfall estimates using the superior instantaneous rain rate estimates obtained from microwave techniques. AGPI, a means of correcting estimation bias for the GPI, is based on adjusting the GPI rain rate with an adjustment ratio (r_a) for each grid:

$$r_a = \frac{V_M}{V_{MIR}} \tag{1}$$

where V_M is the monthly accumulation of instantaneous rainfall estimates for a grid by the microwave technique, and V_{MIR} is the monthly accumulation of instantaneous rainfall estimates for the grid by GPI using the IR data closely coincident with the microwave observations. The adjustment ratio is then applied to adjust the GPI monthly rainfall estimates for the grid calculated with the full hourly IR data. This rainfall adjustment is equivalent to adjusting mean rain rate [*Xu et al.*, 1999]. *Adler et al.* [1993] recommended that V_M and V_{MIR} be smoothed before the calculation of ratio r_a, to

reduce the possible unrealistic large variations of r_a when computed within a relatively small size of grid cell. In this study, an enlarged moving window of 3 × 3 grid cells surrounding the center grid cell is used for the ratio calculation. In addition, the calculated ratio value is restricted within the range of [0.2, 2.0] (also suggested by *Adler et al.* [1994].

3.1.2. UAGPI algorithm. Instead of directly adjusting the rainfall estimates by GPI, this algorithm calibrates the two GPI parameters using microwave rainfall estimates. If R_M denotes the monthly summation of microwave-observed rain pixels for a grid, $N_M(T)$ is the number of IR-estimated rain pixels defined by temperature threshold parameter T and accumulated over the microwave-sampling periods in a month, and $\overline{p}_M$ is the mean microwave-estimated rain rate. Then the optimal IR threshold (T^*) and mean rain rate ($\overline{p}^*$) are calibrated as

$$\mathbf{T}^* = \min_{\mathbf{T}} \left| \mathbf{N}_{\mathbf{M}}(\mathbf{T}) - \mathbf{R}_{\mathbf{M}} \right| \quad (2)$$

$$\overline{\mathbf{p}}^* = \overline{\mathbf{p}}_{\mathbf{M}} . \quad 3)$$

Obviously, $\overline{p}_M$ is derived directly from the microwave observations, and T^* is a product of combining microwave and IR data. It is important to mention that each grid is treated independently and has its own optimal parameters. In essence, UAGPI forces the number of IR-estimated rain pixels to approach that of ground-observed or microwave-observed rain pixels over a month-long period. This is achieved by

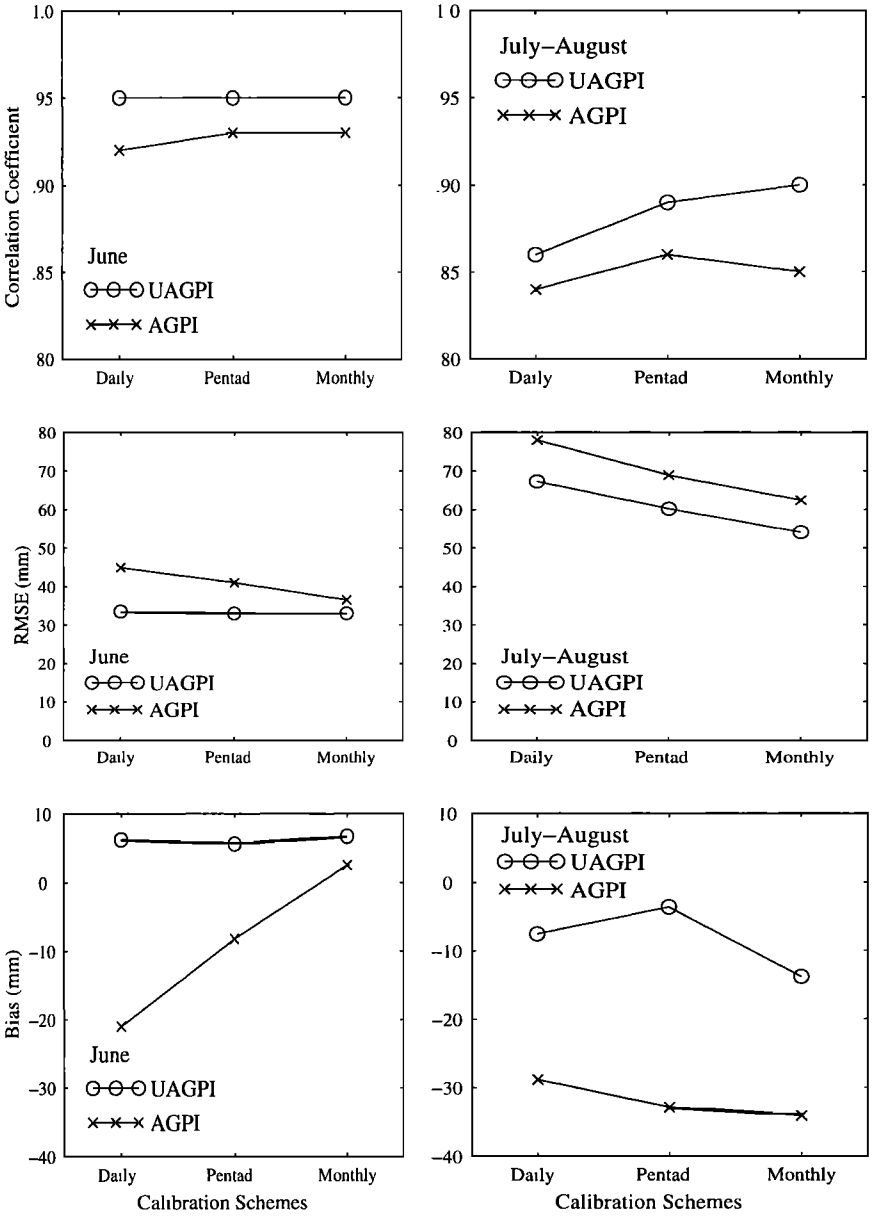

Figure 3. Comparison of monthly rainfall estimates for the June and July/August periods of AIP-1 using universally adjusted GOES Precipitation Index (UAGPI) and adjusted (AGPI) with the daily, pentad, and monthly calibration schemes.

adjusting the IR temperature threshold using microwave rainfall. To be comparable to the application of AGPI, we also used a moving average window of a 3 × 3 grid box in computing the two parameters.

3.2. Calibration Schemes

The AGPI and the UAGPI were all originally proposed for improving GPI rainfall estimates on a monthly temporal scale; therefore the parameters were calibrated on a monthly basis. These algorithms were not generally expected to have the capability of estimating rainfall at higher temporal resolutions. However, changing the monthly calibration scheme may empower them to make rainfall estimates at higher temporal resolutions and keep reasonable accuracy. Monthly, pentad, and daily calibrations for both AGPI and UAGPI algorithms are to be examined,

3.2.1. Monthly calibration. The parameters of GPI are calibrated with microwave rainfall estimates on a monthly basis. Then the single set of the calibrated parameters is applied to all hourly IR observations in a month to compute monthly, pentad, and daily rainfall estimates.

3.2.2. Pentad calibration. The parameters are calibrated for every pentad period for a grid. The computed pentad parameters are then applied to the 5 days for daily and pentad IR rainfall estimates. The monthly estimate is obtained by summing up the daily estimates over the month.

3.2.3. Daily calibration. The parameters are calibrated using only the two microwave observations of a day, and they are applied to the 24-hourly IR observations to make daily rainfall estimates. Then the daily estimates are summed up to obtain pentad and monthly estimates.

4. Results

In addition to examining the results of monthly rainfall estimates by the three calibration schemes, we will also analyze the potential of applying these algorithms for daily and pentad rainfall estimates. The three calibration schemes described above are referred to as the daily, pentad, and monthly schemes, respectively, in the following discussions.

4.1. Rainfall Estimation Over the Japanese Region

To make the rainfall statistics more meaningful, we have eliminated grids with clear sky before computing the statistics. The number of samples for monthly rainfall estimates is 79 for both June and July/August periods. The number of samples for pentad rainfall estimates is 473 for June and 470 for July/August.

Figure 3 shows the variations of three statistics (correlation coefficient, root-mean-square error, and bias) of monthly rainfall estimates for both months using the UAGPI and the AGPI methods with three calibration schemes, respectively. The results demonstrate that the daily calibration scheme can produce as good as or similar monthly rainfall estimates as the monthly calibration for both techniques during the June and the July/August periods. In addition, the pentad scheme produces similar monthly rainfall estimates. When the AGPI calibration scheme was first proposed, a relatively long period and large area were needed for the calibration to produce reasonable values for the ratio [*Adler et al.*, 1993, 1994]. Indeed, the daily calibrated adjustment ratios of the AGPI fluctuated greatly and could not be calculated when the GPI threshold failed to define rain pixels in warm rainfall events (i.e., $V_M \neq 0$ and $V_{MIR} \approx 0$, in equation (1). The adjustment ratios varied from zero to infinity. However, the application of the restriction [0.2, 2.0] substantially limits the fluctuation of the adjustment ratio. The value constraint, although subjective, becomes crucial for applying the AGPI when the adjustment ratio is calibrated on a daily basis. In contrast, the daily calibrated parameters of the UAGPI performed equally well as the monthly calibrated parameters for the monthly rainfall estimates; no restriction is needed for the parameter values. As a result, the two-parameter adjustment of UAGPI makes the IR rainfall samples physically more similar to the coincident microwave rainfall samples than the adjustment of AGPI. Even with the value constraint, the AGPI performed poorer than the UAGPI in all three parameter calibration schemes for monthly rainfall estimates during both months. Specifically, the monthly rainfall estimates by the UAGPI have greater correlation coefficients, lower root-mean-square errors, and lower absolute biases than those corresponding statistics computed from rainfall estimates by the AGPI for all three calibrating schemes. Figure 4 shows the scatterplots of monthly rainfall estimates by the UAGPI and the AGPI using daily calibrated parameters for both the June and the July/August periods. The better monthly statistics in June (as compared to those for July/August) demonstrated that combining techniques like the UAGPI and the AGPI performed better for the bai-u frontal rainfall regime than for convective regime because of the large temporal and spatial scales of the former.

The results of pentad rainfall estimates using the UAGPI and the AGPI are shown in Figure 5. When the statistics were computed, a pentad rainfall estimate on each grid was considered as an independent sample. For example, during the 30 days of the June period over the study area which contained 79 grids of 1.25° × 1.25°, there were 79 x 6 independent samples. Those samples corresponding to 5-day clear skies, however, were not used for the computation of these three statistics in order to emphasize the estimates during cloudy periods. As indicated in Figure 5, the pentad rainfall estimates using daily and pentad-calibrated parameters had similar statistics for the UAGPI and the AGPI during both months. The ranges of these statistics clearly demonstrate that the pentad rainfall estimates by these algorithms had a high degree of accuracy, if the microwave can provide accurate rainfall measurements twice a day. The monthly scheme, however, performed poorer than the other two calibration schemes because the monthly calibration could not catch the parameter variations in each pentad period. Again, the UAGPI produced better statistics in pentad rainfall estimates than the AGPI did for both daily and pentad-calibration schemes in both months. Figure 6 shows the scatterplots of pentad rainfall estimates using daily calibrated parameters by these two algorithms. Similar to the statistics of monthly rainfall estimates discussed above, the statistics of pentad-rainfall estimates for the June period were better than those for the July/August period, implying the more severe sampling deficiency of microwave observations for the convective rainfall regime than for the frontal rainfall regime.

It is generally believed that the sparse sampling of microwave observations may provide insufficient information to the AGPI and UAGPI calibration schemes if these algorithms are applied to daily rainfall estimates. In other

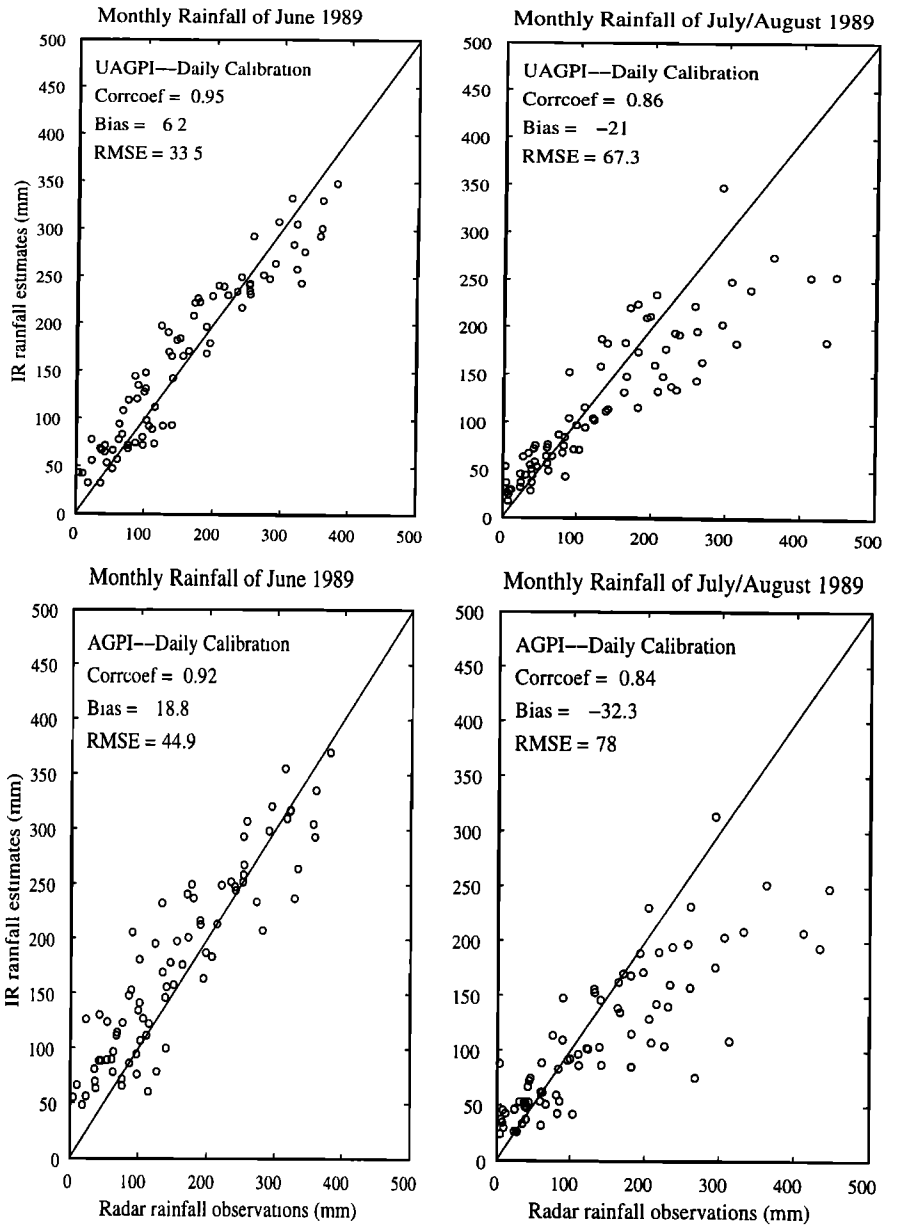

Figure 4. Scatterplots of monthly rainfall estimates of UAGPI and AGPI using daily calibration scheme for the June and July/August periods of AIP-1 versus ground observations.

words, given the twice-a-day microwave observations, neither AGPI nor UAGPI is able to produce reliable daily rainfall estimates. However, the examination of daily rainfall estimates by the UAGPI and the AGPI would further reveal merits and limitations of these algorithms and indicate the possible directions of improvements for these algorithms. Because the variations of model parameters on a daily basis cannot be represented by parameters computed from a longer calibration period (as indicated in the previous paragraph), we only examine the daily rainfall estimates using a daily scheme.

Figures 7 and 8 show the correlation coefficients, root mean-square-errors (RMSE), and biases of the UAGPI and the AGPI daily rainfall estimates over the Japanese region, respectively. These statistics were computed for each grid using the daily samples over a month. Therefore there are 79 computed values for each statistic corresponding to the 79 grid cells in the study area. We illustrated these statistics in their histograms, showing their value distributions. The daily rainfall estimates by the UAGPI had a high degree of correlation with the radar-gage composite in both months, while the correlation coefficients by the AGPI were much weaker. Specifically, the correlation coefficients by the UAGPI are around 0.9 in the June period and concentrate in the range of [0.7, 1.0] during the July/August period. For both the UAGPI and the AGPI techniques, the RMSE of daily rainfall estimates in June have smaller values and a narrower range of distribution than those values in the July/August period. In addition, the biases are more concentrated around zero in June than those in July/August. Overall, daily rainfall

estimates are more accurate in June than those in July/August, and the UAGPI performed better than the AGPI for the daily rainfall estimation. Consequently, it is tentatively inferred that when accurate twice-a-day observations of instantaneous rainfall are available, the combining techniques like UAGPI are able to produce more reliable daily rainfall estimates for frontal rain regimes than for convective rain regimes.

4.2. Rainfall Estimation Over the Tropical Area

As was done for AIP-1 data, grids with clear sky were not used for computing the rainfall statistics for AIP-3 data. The number of samples for monthly rainfall estimates is 26, for pentad rainfall estimates is 154, and for daily rainfall estimates is 638.

Figure 9 shows the variation of statistics for monthly, pentad, and daily rainfall estimates by the UAGPI and AGPI using three calibration schemes. The rainfall estimates were computed on grids of $1° \times 1°$ within full or partial coverage by the two ship-borne radar. Because the number of the grids within the study area is relatively small, the statistics were computed using radar rainfall observations and IR rainfall estimates in both month 2 and month 3 of the intensive experiment period. For example, two independent samples of accumulated monthly rainfall from both cruises on each radar-covered grid are accounted for calculating statistics of monthly rainfall estimates. Similarly, independent samples of pentad rainfall estimates were also derived from both months for the computation of pentad statistics. The statistics of daily rainfalls were calculated through all grid cells within the

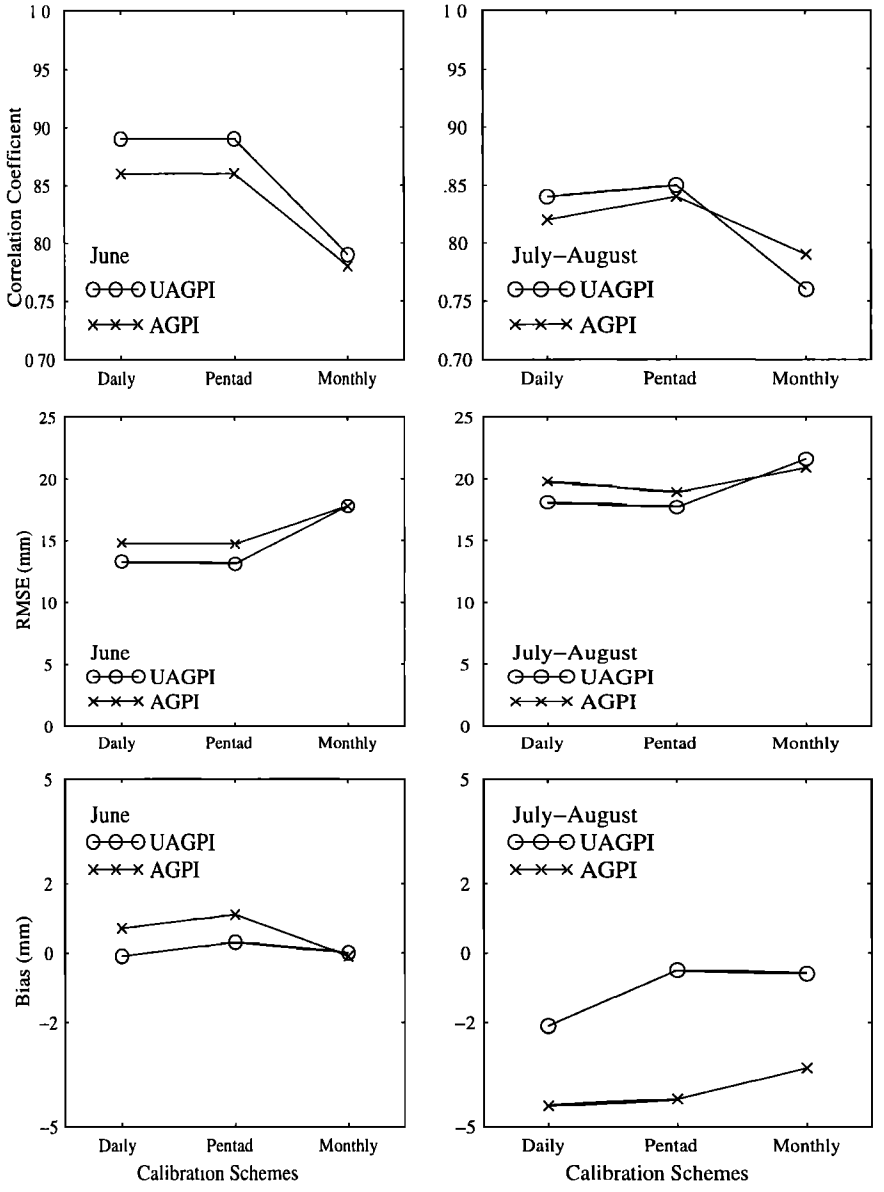

Figure 5. Comparison of correlation coefficients, root-mean-square errors, and biases of pentad rainfall estimates for the June and July/August periods of AIP-1 using UAGPI and AGPI with the daily, pentad, and monthly calibration schemes.

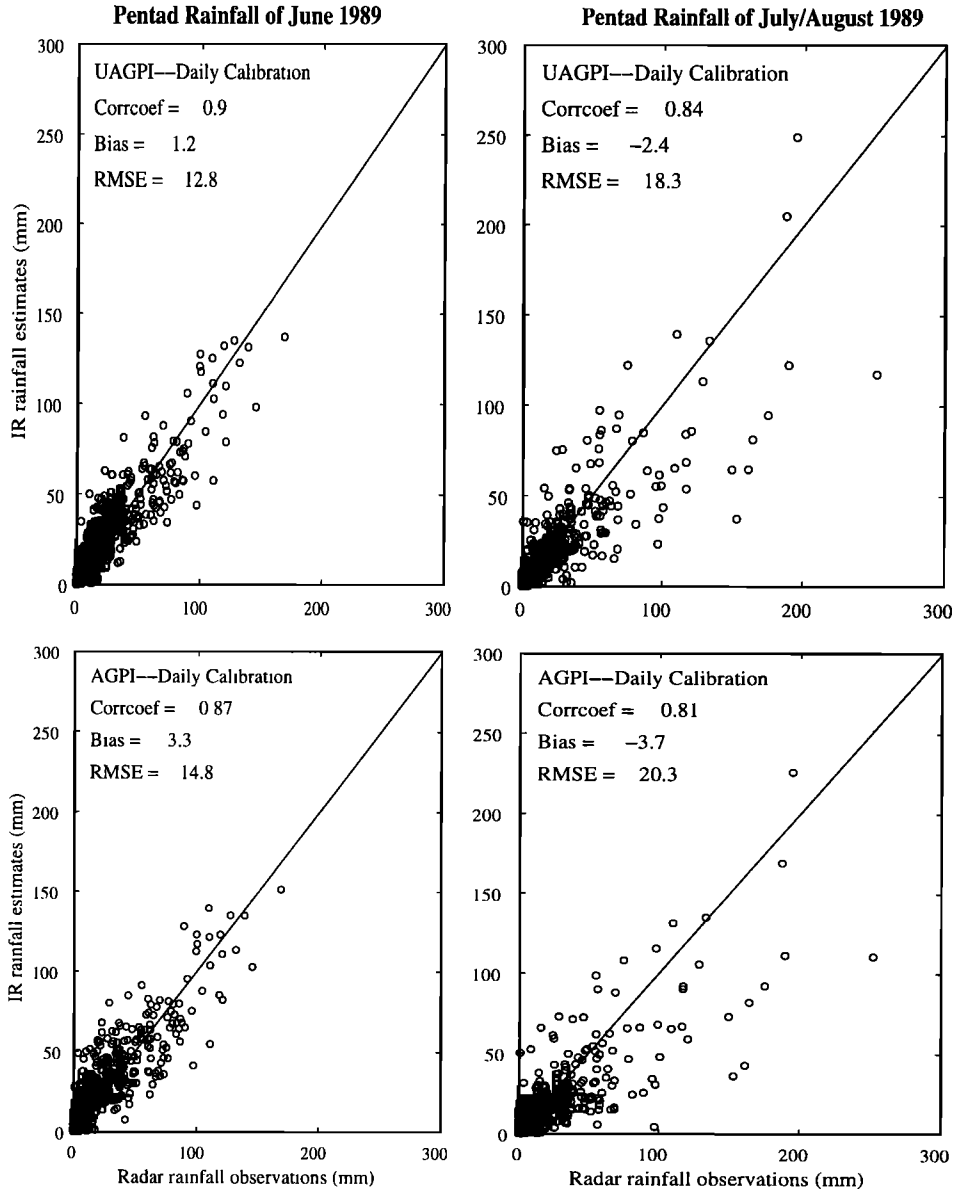

Figure 6. Same as Figure 4 but for pentad rainfall estimates.

study area and for both months, because of the small size of the radar-covered region. Grids that had daily and pentad-long clear skies were also eliminated before those statistics were computed.

Overall, the rainfall estimates by the UAGPI and AGPI produced similar statistics on the temporal scale of monthly, pentad, and daily when pentad and monthly calibration schemes were used. For the AGPI the daily scheme performed generally poorer than the other two schemes in rainfall estimates of all three temporal scales, while the daily scheme performed as good as the other two schemes for the UAGPI. In addition, the statistics of the pentad scheme were as good as those derived from the daily scheme and consistently better than those derived from the monthly scheme when the UAGPI was applied. In particular, the statistics of monthly rainfall using monthly calibrated parameters are consistently poorer than the corresponding statistics using pentad-calibrated parameters for both AGPI and UAGPI techniques. These results demonstrated that the daily calibration period is not long enough to produce stable adjustment ratios for the AGPI over the tropical region. On the other hand, the monthly scheme over smoothed the parameters so that they were unable to capture the variation of these parameters. In general, the rainfall estimates by the AGPI were as good as those by the UAGPI when the pentad scheme was used for parameter calibration. Most rainfall events in the AIP-3 data sets were associated with clouds whose tops were colder than 235°K measured in IR brightness temperature. In comparison with the Japanese region the correlation coefficients of the rainfall estimates over the tropical area were poorer; they fell in the range of 0.8-0.9 for monthly rainfall estimates and 0.6-0.7 for pentad estimates. The poorer performances over the tropical region indicate that the twice-a-day rain measurements may be insufficient in applying these algorithms for rainfall

estimates with temporal resolutions higher than monthly. One should, however, be careful in interpreting the results, because the partial radar coverage on a majority of the grids over the AIP-3 region, and the difference in the quality of radar observations of these two data sets [*Ebert et al.*, 1996], may contribute considerably to the different performances.

In summary, with the availability of accurate twice-a-day instantaneous rain observations, both the UAGPI and the AGPI are able to produce high-quality monthly and relatively reliable pentad-rainfall estimates using AIP-1 and AIP-3 data sets. The performance of the AGPI, however, depends highly on the condition of the majority of rain events associated with clouds with top temperatures colder than 235°K. In addition, a restriction on the values of the adjustment ratio is crucial for the AGPI technique to produce useful rainfall estimates. The UAGPI showed promisingly potential for daily rainfall estimates. Overall, the daily scheme performed generally as good as the other two schemes in rainfall estimation at monthly, pentad, and daily temporal scales.

5. Sampled Rain Area and Estimation Error

In this section the relationship between the rain area sampled by polar-orbiting microwave sensor and the rainfall estimation error is analyzed further using the daily calibration scheme with the AIP-1 data set. This analysis explores the potentials of the UAGPI in rainfall estimation and the directions of its improvements.

Physically, the quality of the calibrated GPI parameters depends on the rain area detected by the satellite microwave

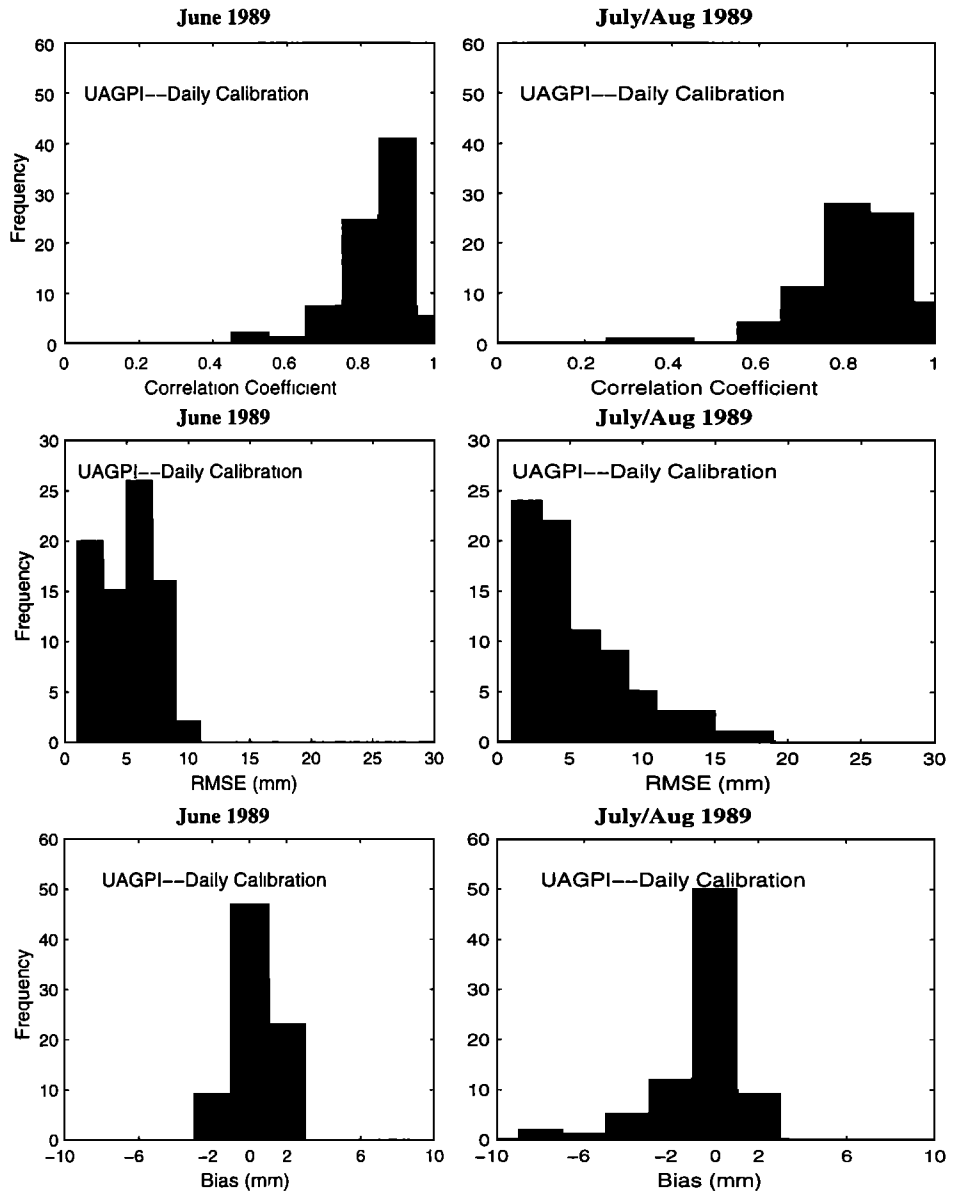

Figure 7. Histogram of correlation coefficients, root mean square errors, and biases of daily rainfall estimates for the June and the July/August periods of AIP-1 using UAGPI with the daily calibration scheme.

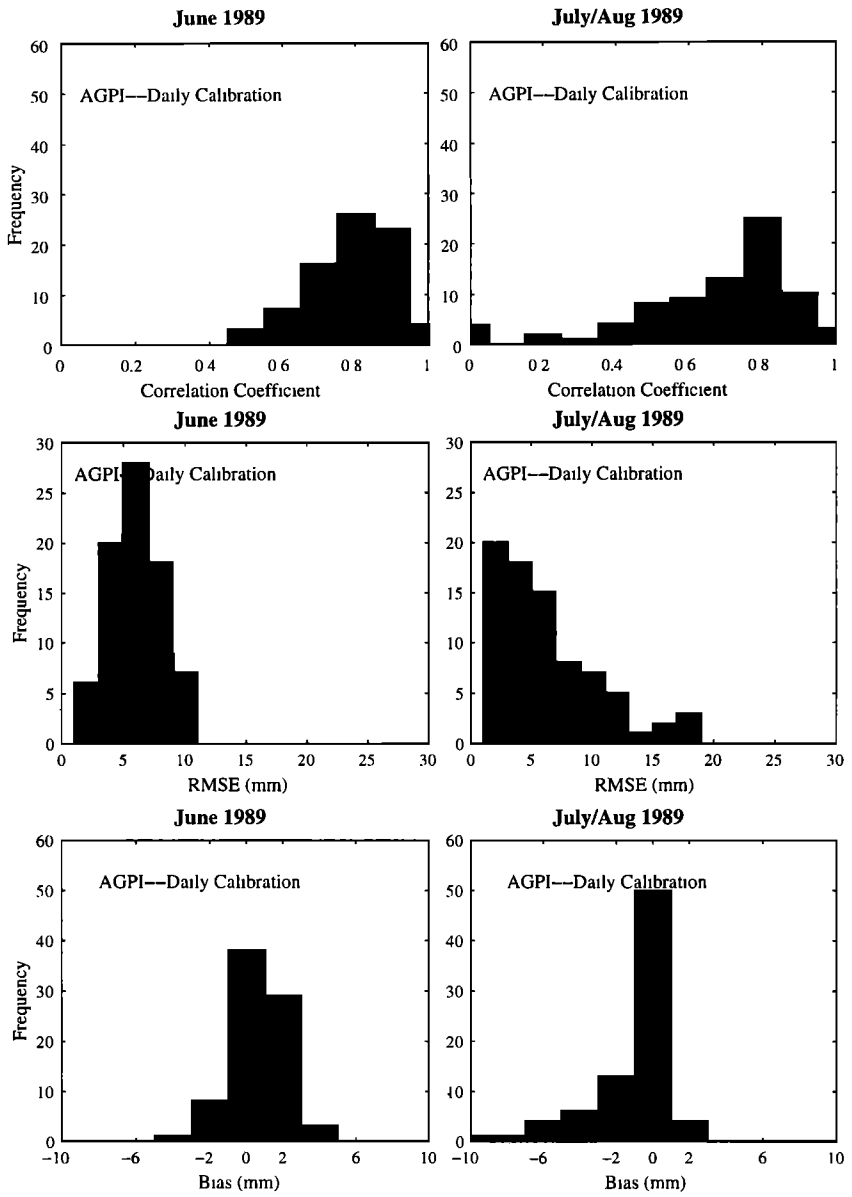

Figure 8. Same as Figure 7 but using AGPI.

observations, because the rain area is a very effective factor describing the rainfall field [*Chiu,* 1988], and the GPI parameters are calibrated locally on all grids. Specifically, the quality of the GPI parameters is directly a function of the deviation of microwave-detected daily rain area from the actual accumulated rain area measured by radar-gage composites over a day. To describe this deviation, we designed the detection rate of the daily rain area (β) as follows:

$$\beta = \frac{A_M}{A_T} \quad (4)$$

where A_M is the microwave-detected daily rain area, and A_T is the real daily rain area. Specifically, A_M is the geometric union of two hourly rain fields measured by microwave observations, and A_T is the geometric union of hourly rain fields of the radar-gage composites. Because we have used the radar-gage composites to simulate the microwave rain observations in this research, the detection rate falls in the range of [0, 1], where the value 1.0 designates the case of perfect detection, and zero is for the complete failure of rain detection by microwave data. The detection rate is affected mainly by two factors for a rain regime: sampling rate of microwave observations and the movement and variation of the rain system over time. Figure 10 shows the histograms of the daily detection rate for both the June and July/August periods, and clear days were not included in the histograms. In general, the detection rates are greater for the bai-u frontal-dominated June than those for the subtropical convectives which prevailed in the July/August.

To examine the effects of the detection rates on rainfall estimation, we related the detection rates to the corresponding proportional root square errors (PRSE) of daily rainfall estimates over the whole study region. The PRSE (E_d) is defined as follows:

$$E_d = \frac{\sqrt{\sum_{i=1}^{N}(R_i^e - R_i^o)^2}}{\sum_{i=1}^{N} R_i^o} \quad (5)$$

where R_i^e is the daily IR rainfall estimate on grid i, and R_i^o is the daily rainfall of the radar-gage composite. Because the daily RMSE is generally proportional to the total daily rainfall volume over the study area, the PRSE is considered more directly related to the parameters used in the UAGPI method. The correlation between the detection rate and the PRSE certainly reveals the relationship between the accuracy of the calibrated parameters and the detection rate. Figure 11 shows the scatterplots of the detection rate and PRSE for both the June and the July/August periods. The correlation coefficient for June is –0.77 and is –0.69 for the July/August period. This high negative correlation demonstrates that the detection rate is an obvious determinant to the quality of calibrated GPI parameters, which in turn determine the accuracy of rainfall estimates. In other words, the model parameters cannot be adequately calibrated over the poorly detected rain area. Obviously, increasing the sampling rate of microwave observations would be a direct way to increase the detection rate and improve the rainfall estimation. The study of current microwave sampling deficiency for daily rainfall estimation using the UAGPI technique would benefit substantially from further research using TRMM microwave rain estimates over tropical and subtropical regions.

6. Conclusions

Three schemes of calibrating parameters for the UAGPI and the AGPI have been examined using the AIP-1 and the

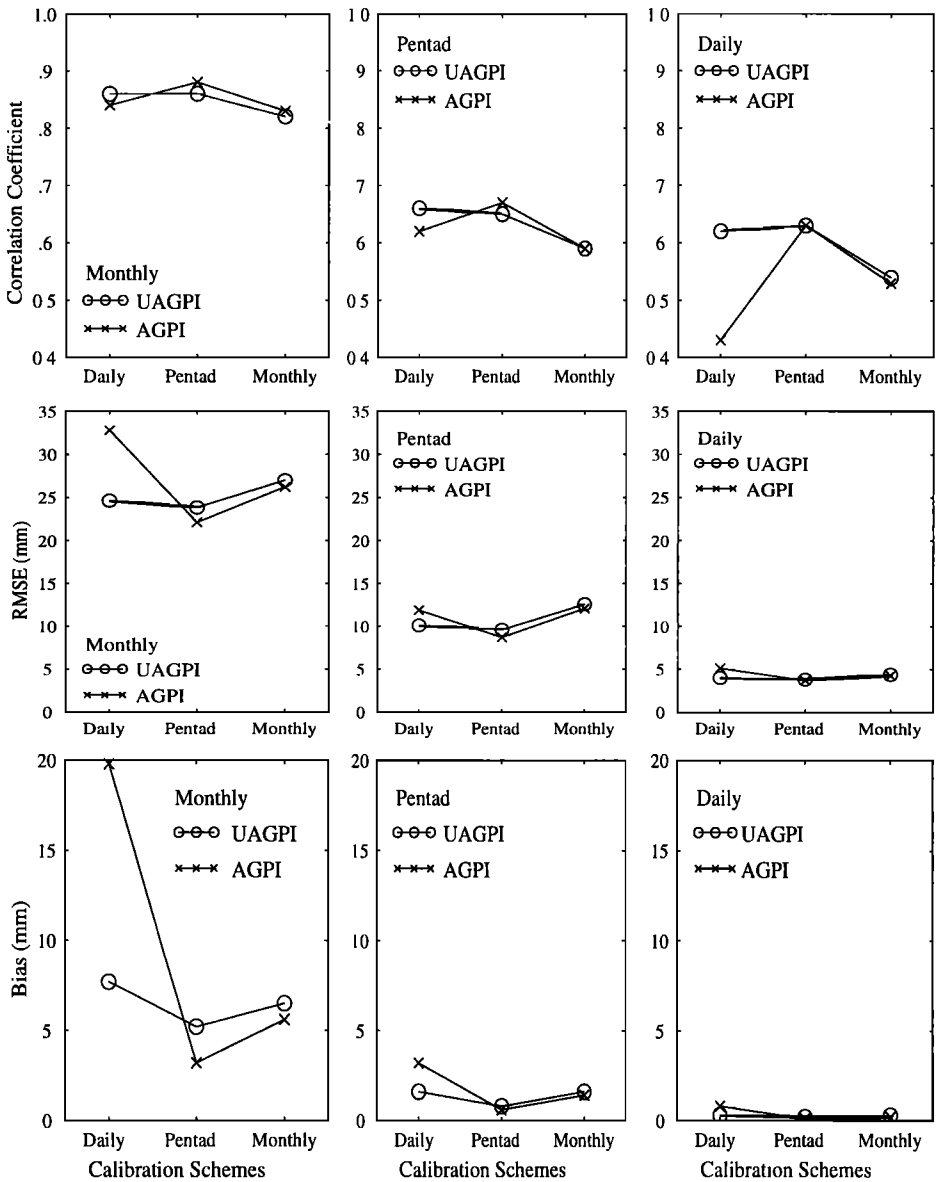

Figure 9. Same as Figure 5 but for the AIP-3 data set.

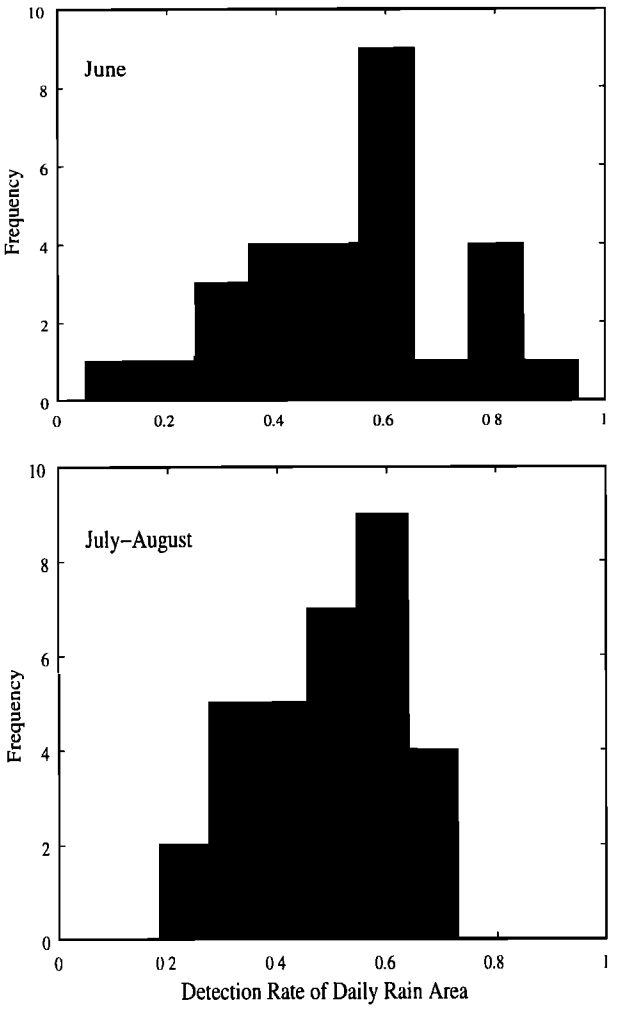

Figure 10. Histograms of the detection rate of rain areas for both the June and the July/August periods of AIP-1.

AIP-3 data sets for daily, pentad, and monthly rainfall estimates. These schemes are daily, pentad, and monthly calibrations, which are named in terms of their calibration periods. Microwave rain observations were simulated with the radar-gage composite to study the effects of calibration schemes on the estimation errors associated with the insufficient sampling rate of polar-orbiting satellites. In general, the comparison of these three schemes in both data sets showed that the parameter calibration period should match the temporal scales of rainfall estimates for the applications of these algorithms. However, the results of the AIP-1 data sets clearly demonstrated that the parameters from the daily and pentad calibration schemes were able to produce as good as or similar monthly rainfall estimates as the parameters from the monthly scheme. This was still true for the UAGPI when the AIP-3 data set was used. Overall, the combination techniques performed better for the bai-u frontal rain regime (June) than for the convective storms (July/August) using the AIP-1 data set. The UAGPI generally performed better than the AGPI with three calibration schemes examined. Consequently, when the AGPI and UAGPI techniques are applied for rainfall estimates on climatic scales, the pentad scheme is suggested for the monthly, pentad, and daily rainfall estimates to possess more samples from the polar-orbiting microwave observations, especially for the convective rainfall systems.

To describe the relationship between the sampling rate of microwave observations and the error of rainfall estimation, we defined the detection rate of the daily rain area, which is determined directly by the sampling rate. The results of the AIP-1 data set showed the high negative correlation between the detection rate and the PRSE of daily rainfall estimates. This indicates that increasing the detection rate is an effective way of reducing the estimation error due to the localization of the parameter calibration. Yet, the detection rate increase requires the increase of the sampling rate of microwave observations, which is not applicable for the currently operational meteorological satellites. Another promising way of reducing estimation error is to adjust the calibrated parameters over time and space by following the movement and variation of a rain regime.

In addition to comparing various parameter calibration schemes, this research has shown that with some modifications, the UAGPI is also a promising algorithm for daily rainfall estimates on large spatial scales. TRMM data will be used to test the primary results of this research about various calibration schemes and to further improve the UAGPI for daily rainfall estimation.

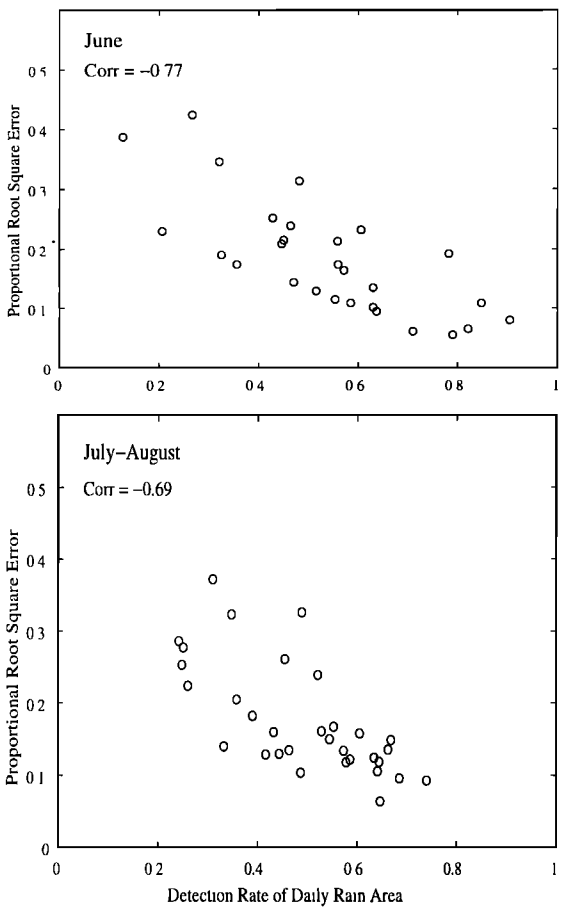

Figure 11. Scatterplots of the detection rate of rain areas and the proportional root-square-error for the June and the July/August periods of AIP-1.

Acknowledgments. The authors would like to gratefully acknowledge the support provided by the NASA's EOS-IDS grant NASA NAG5-3640 and TRMM grant NASA NAG5-7716.

References

Adler, R. F., A. J. Negri, P. R. Keehn, and I. M. Hakkarinen, Estimation of monthly rainfall over Japan and surrounding waters from a combination of low-orbit microwave and geosynchronous IR data, *J. Appl. Meteorol., 32*, 335-356, 1993.

Adler, R. F., G. J. Huffman, and P. R. Keehn, Global rain estimates from microwave adjusted geosynchronous IR data, *Remote Sens. Rev., 11*, 125-152, 1994.

Arkin, P. A., The relationship between fractional coverage of high cloud and rainfall accumulations during GATE over the B-scale array, *Mon. Weather. Rev., 107*, 1382-1387, 1979.

Arkin, P. A. and P. E. Ardanuy, Estimating climatic-scale precipitation from space: A review, *J. Clim., 2*, 1229-1238. 1989.

Arkin, P. A. and B. N. Meisner, The relationship between large-scale convective rainfall and cold cloud over the Western Hemisphere during 1982-84, *Mon. Weather. Rev., 115*, 51-74, 1987.

Arkin, and P. Xie, The global precipitation climatology project: First algorithm intercomparison project. *Bull. Am. Meteorol. Soc., 75*, 401-419, 1994.

Chiu, L. S., Estimating areal rainfall from rain area, in *Tropical Rainfall Measurements*, edited by J. S. Theon and N. Fugono, pp. 361-367, A. Deepak, Hampton, Va., 1988.

Ebert, E. E., M. J. Manton, P. A. Arkin, R. J. Allam, G. E. Holpin, and A. Gruber, Results from the GPCP algorithm intercomparison programme, *Bull. Am. Meteorol. Soc., 77*, 2875-2886, 1996.

Ferraro, R. R., and G. F. Marks, The development of SSM/I rain-rate retrieval algorithms using ground-based radar measurements, *J. Atmos. Oceanic Technol., 12*, 775-770, 1995.

Huffman, G. J., R. F. Adler, P. Arkin, A. Chang, R. Ferraro, A. Gruber, J. Janowiak, A. McNab, B. Rudolf, and U. Schneidar, The global precipitation climatology project (GPCP) combined precipitation data set, *Bull. Am. Meteor. Soc., 78*, 5-20, 1997.

Lee, T. H., J. E. Janowiak, and P. A. Arkin, Atlas of products from the algorithm intercomparison project, 1, Japan and surrounding oceanic regions June-August 1989, 131 pp., Univ. Corp. for Atmos. Res., Boulder, Colo., 131 pp., 1991.

Simpson, J., C. Kummerow, W.-K. Tao, and R. F. Adler, On the Tropical Rainfall Measuring Mission (TRMM), *Meteorol. Atmos. Phys., 60*, 19-36, 1996.

Xu, L., Estimating rainfall from satellite infrared imagery: Cloud patch analysis, Ph.D. dissertation, Dep. of Hydrol. and Water Resour., Univ. of Ariz., Tucson, 1997.

Xu, L., X. Gao, S. Sorooshian, P. A. Arkin, and B. Imam, A microwave infrared threshold technique to improve the GOES Precipitation Index, *J. Appl. Meteorol., 38*, 569-579, 1999.

X. Gao, B. Imam, S. Sorooshian, and L. Xu, Department of Hydrology and Water Resources, University of Arizona, Tucson, AZ 85721-0011. (bisher@hwer.arizona.edu; gao@hwr.arizona.edu; soroosh@hwr.arizona.edu; Liming@hwr.arizona.edu.)

(Received July 20, 1999; revised December 17, 1999;
accepted January 4, 2000.)